Available online at www.sciencedirect.com
SCIENCE DIRECT®
Physica C 411 (2004) 11–17
PHYSICA C
www.elsevier.com/locate/physc

Huge compact flux avalanches in superconducting Nb thin films

M.S. Welling *, R.J. Westerwaal, W. Lohstroh, R.J. Wijngaarden

Division of Physics and Astronomy, Faculty of Sciences, Vrije Universiteit, De Boelelaan 1081, 1081HV Amsterdam, The Netherlands

Received 1 June 2004; received in revised form 15 June 2004; accepted 21 June 2004

Abstract

Using a magneto-optical technique we perform a quantitative analysis of magnetic flux penetration in superconducting niobium thin films on *A*-plane $(1\,1\,\bar{2}\,0)$ sapphire substrates as a function of temperature ($1.5\ \mathrm{K} \leqslant T \leqslant T_c = 9.2\ \mathrm{K}$). In these samples we observe huge compact avalanches (HCAs for brevity), very much like some snow-avalanches and unlike the rough dendritic flux penetration observed on *R*-plane $(1\,\bar{1}\,0\,2)$ sapphire. The behavior observed is consistent with the occurrence of thermo-magnetic avalanches as proposed by Aranson et al. [Phys. Rev. Lett. 87 (2001) 067003]. For increasing temperature, we find: (1) an increased branching of the HCA. (2) An increased applied field necessary for the first HCA to occur. (3) A decrease in the number of HCAs, accompanied by more 'regular' flux penetration (above 6.2 K avalanches are completely absent). (4) An increase of the total amount of flux as well as the area of the HCA.
© 2004 Elsevier B.V. All rights reserved.

PACS: 45.70.Qj; 45.70.Ht; 74.78.Db; 74.25.Ha; 74.25.Qt; 68.55.Jk
Keywords: Flux jump; Avalanche; Thin film; Niobium; Superconductor; Magneto-optical imaging

1. Introduction

Catastrophic flux penetration was already reported by Huebener et al. [1], one of the pioneers in the field of magneto-optical investigations on flux penetration behavior in superconductors. The avalanches of magnetic flux can move extremely fast and have been observed in a number of superconductors like Nb [1], MgB_2 [3–5] and $YBa_2Cu_3O_{7-x}$ films [2].

In this paper we focus on niobium, where avalanches previously have been observed using scanning Hall probe microscopy (SHM) [6], Hall probe arrays [7–9], and magneto-optical imaging [1,9–12].

Interestingly, different authors [1,6,9–11] have reported quite different flux penetration behavior for superconducting niobium. Some authors report smooth [1] and regular Bean-like [13] flux penetration but also seaweed-like patterns [1,12]

* Corresponding author. Tel.: +31 20 4447923; fax: +31 20 4447992.
E-mail address: welling@nat.vu.nl (M.S. Welling).

0921-4534/$ - see front matter © 2004 Elsevier B.V. All rights reserved.
doi:10.1016/j.physc.2004.06.011

are observed, whereas others find rather irregular, 'rough' Bean-like flux patterns [6]. In a previous publication [15] we showed that such rough flux penetration takes place in niobium thin films on *R*-plane sapphire substrates and that it can be changed into a more fractal, tree-like pattern by exposing the niobium to hydrogen.

Here, we present a systematic magneto-optical (MO) study of the burst-like magnetic flux penetration in superconducting niobium thin films on *A*-plane $(1\,1\,\bar{2}\,0)$ sapphire substrates. Such compact and burst-like flux penetration behavior is possibly of thermo-magnetic origin [3,14]. Since vortex motion causes local heating, pinning then is reduced enabling further flux motion. This can cause a macroscopic amount of flux to suddenly invade the superconductor. Support for such thermo-magnetic avalanches is obtained from numerical simulations of coupled differential equations for the magnetic induction B and temperature T [14]. Here we perform an experimental quantitative analysis on individual huge compact avalanches (HCAs for brevity) as a function of applied magnetic field and temperature ($1.5\ \mathrm{K} \leqslant T \leqslant T_c = 9.2\ \mathrm{K}$).

This paper is organized as follows. In Section 2 we briefly discuss the sample and the experimental procedure as well as the MO set-up. In Section 3.1, we show the influence of the temperature on the magnetic field distribution. In Section 3.2, we compare the present results with those on samples on *R*-plane $(1\,\bar{1}\,0\,2)$ sapphire substrates. We end with a summary of the main results and a discussion in Section 4.

2. Experimental

For our magneto-optical study we use niobium thin films of 500 nm thickness, which are evaporated at 973 K under ultra high vacuum (UHV) conditions (base pressure 2×10^{-7} Pa) on *A*-plane $(1\,1\,\bar{2}\,0)$ sapphire substrates. During evaporation a shadow mask is used to obtain a strip geometry of $9.0\times1.8\ \mathrm{mm}^2$. Hereafter, we evaporated at room temperature a thin Pd layer, 10 nm thick, on top of the niobium layer to protect the sample from oxidation and to be able to investigate the influence of hydrogen on the flux penetration behavior as discussed elsewhere [15] (in this reference also more results of sample characterization are given).

In our experiments we measure the local magnetic flux density (B_z) immediately above the superconducting sample using a magneto-optical image lock-in amplifier [16]. To sense the magnetic field a Bi-substituted ferrite–garnet film [17] is used with in-plane magnetization vector and large Faraday effect (typically 0.06 deg/mT). This 'indicator' is mounted on top of the sample. The assembly consisting of sample and indicator is mounted in a specially built cryogenic polarization microscope, which fits into the variable temperature insert of an Oxford Instruments 1 T magnet system. The externally applied magnetic field is perpendicular to the sample and indicator surface. Experiments are performed after zero field cooling (ZFC) to 1.5 K, and from 4.2 K to $T_c = 9.2$ K in steps of 0.5 K. Furthermore, we repeated the experiments at 4.2 and 6.7 K three times to investigate the reproducibility. In each of these experiments the sample is cooled down in zero field, subsequently the externally applied magnetic field is increased from 0 to 40 mT in steps of 100 μT, using a constant sweep rate of 100 μT/s between steps. After every field step, the flux distribution in the sample is relaxed for 9 s after which a MO image is acquired. Only the central part of the strip is investigated to avoid geometrical effects due to the corners. Pictures are taken using a charge-coupled device camera (with 782×582 pixels) with an exposure time of 350 ms. Spatial resolution is such that one side of the square pixel corresponds to 3.4 μm.

3. Results

3.1. Effect of temperature

In Fig. 1 we show magnetic flux distributions for various temperatures. For every image, we applied a magnetic field of 40.0 mT after zero field cooling. The Meissner phase appears black and the Shubnikov phase bright. Fig. 1a shows the magnetic field pattern at 1.5 K, where we observe finger-shaped instantaneous bursts (on our experi-

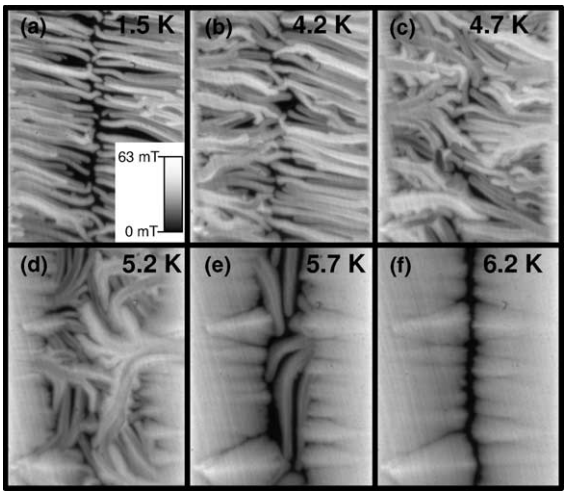

Fig. 1. Magnetic flux distribution in a 500 nm Nb thin film on an *A*-plane sapphire substrate after zero field cooling and subsequently applying a field of 40.0 mT at the temperature indicated. The scale-bar indicates the local magnetic field B_z and holds for all figures (a)–(f).

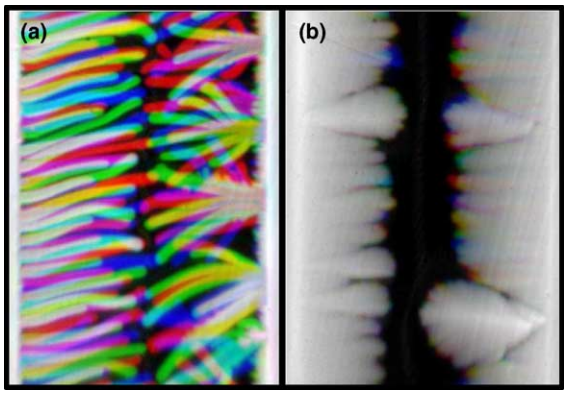

Fig. 2. Overlapping images in red, green, and blue for three identical experiments, where after zero field cooling a magnetic field of 20 mT is applied. (a) At 4.2 K we observe colors indicating that the HCAs do not reproduce at the same positions. (b) At 6.7 K, no HCAs occur and flux penetration is much more reproducible. However, different colors correspond to small avalanches that also do not reproduce.

mental time scale, limited by our camera) of magnetic flux entering the superconductor. At 4.2 K (Fig. 1b), the magnetic field pattern appears slightly more irregular. At 4.7 K (Fig. 1c), we observe more branching and more irregular and larger HCAs. At 5.2 K, (Fig. 1d), in addition to the HCAs a more regular flux penetration behavior dominates at the edge of the sample. At 5.7 K, (Fig. 1e), few, but very large and branched HCAs are observed. At 6.2 K and above (Fig. 1f), no HCAs are observed anymore: flux penetrates in a regular manner.

To show that the flux penetration behavior caused by HCAs is not reproducible on a detailed level, we show in Fig. 2a as a color image the superposition of images from three experiments at the same temperature of 4.2 K indicated by red, green, and blue, respectively. Consequently, if the flux penetration behavior would reproduce exactly we would observe a black and white only image, since red, green, and blue in all images would overlap. As follows directly from the colors in Fig. 2a, the HCAs do not reproduce. Consequently, this flux penetration is not trivially determined by e.g. a macroscopic defect but by an intrinsic instability [14], that is sensitive to the exact initial conditions (e.g. the exact flux distribution, distribution of pinning sites and thermal noise). At 6.7 K, as shown in Fig. 2b, no HCAs are observed, indicating the disappearance of the instability.

In Fig. 3a–c we show the dramatic influence of a particular but representative HCA on the magnetic flux distribution at 5.7 K as a three-dimensional plot: (a) at 21.4 mT before the HCA and (b) at 21.5 mT, after the avalanche. To show the subsequent evolution of the flux penetration, Fig. 3c presents the flux distribution at 33.0 mT. In Fig. 3d we show the magnetic field profiles B_z along the white lines of Fig. 3a–c. The significant zchange in the profile from before the HCA (squares) and after (thick line) can be clearly observed. While the profile before the avalanche is Bean-like [13], after the occurrence of the HCA it is almost constant. This remarkable feature, that B_z is more or less constant along the center of the HCA, is observed for many of the early HCAs (when at low applied field they are not yet overlapping with each other). The profile in open circles shows that with further increase of the external field, the slope of the profile in the vicinity of the edge is recovered: a new Bean-like profile develops on top of the avalanche.

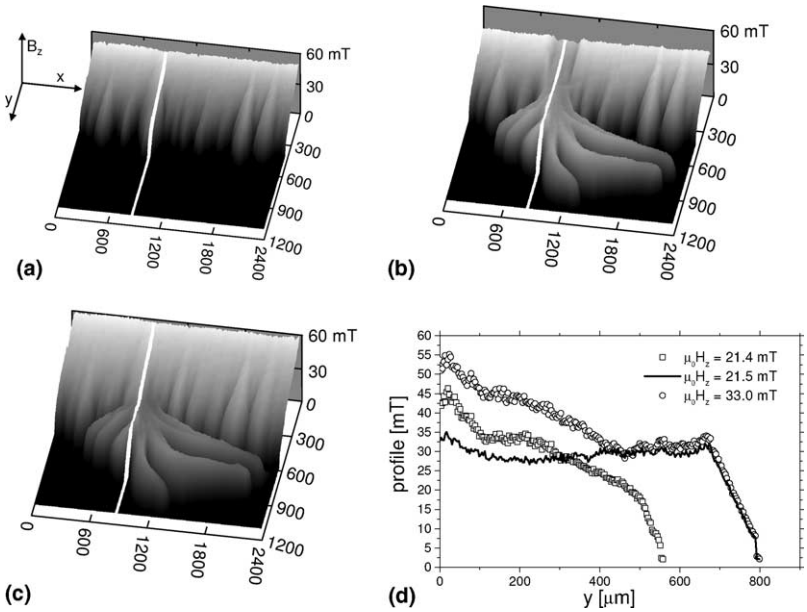

Fig. 3. Three-dimensional plots of magneto-optical measurements at 5.7 K showing the dramatic change of the magnetic flux distribution by a single HCA, (a) before the HCA at 21.4 mT, (b) after the HCA at 21.5 mT. Note that the magnetic flux landscape is annealed by the HCA even at the edge. (c) Field distribution at 33.0 mT showing that the further progress of the flux penetration fills the 'mountain pass' at the edge. (d) Profiles of the magnetic field along the white lines indicated in figures (a)–(c). Before the HCA, we observe a monotonic slope (squares) corresponding to a Bean profile. After the occurrence of the HCA, the profile becomes almost constant (line). With further increase of the external field a new Bean profile develops 'on top' of the avalanche (circles).

We now turn to a quantitative analysis of the HCAs in the temperature range ($1.5\ \mathrm{K} \leqslant T \leqslant 5.7\ \mathrm{K}$). The data analyzed is from a series of five experimental runs, each consisting of ~400 field steps. The size and shape of the *individual* avalanches was determined from the difference $\Delta B_z(x,y)$ of two consecutive images. We binarize this difference image using a threshold value of 10 mT resulting in an (binary) image of the active areas participating in the avalanches. Thus we identify the area A covered by an *individual* HCA. Subsequently, the size S expressed as the total magnetic flux participating in a particular avalanche, is calculated from

$$S = \int_A |\Delta B_z(x,y)| \, \mathrm{d}x\mathrm{d}y. \tag{1}$$

Thus for every HCA we obtain the area A and the size S of the avalanche. In the following we shall show that the area of the HCA increases with increasing temperature. However, also S is found to increase with temperature. We find that the *ratio* S/A, which is the average field $\langle B_z \rangle_{\mathrm{HCA}}$ of the HCA is roughly independent of temperature. To show this we plot in Fig. 4a the average magnetic induction of all observed HCAs at various temperatures. Since in one single magnetic field step several HCAs can occur, which we identify as separate events, we plot along the x-axis the avalanche index. Clearly, independent of temperature $\langle B_z \rangle_{\mathrm{HCA}}$ appears to fluctuate around an average value of ≈21 mT (see also Fig. 4b) indicated by the thin horizontal line. Note that with increasing temperature, the number of HCAs decreases from almost 100 events at 1.5 K to just 3 at 5.7 K. In Fig. 4b for each temperature, the average magnetic induction $\langle B_z \rangle_{\mathrm{ALL}}$ over all HCAs is plotted. Note that deviations from a constant value for $\langle B_z \rangle_{\mathrm{ALL}}$ set in above 5.5 K, where also the qualitative behavior is changing very much and only few ava-

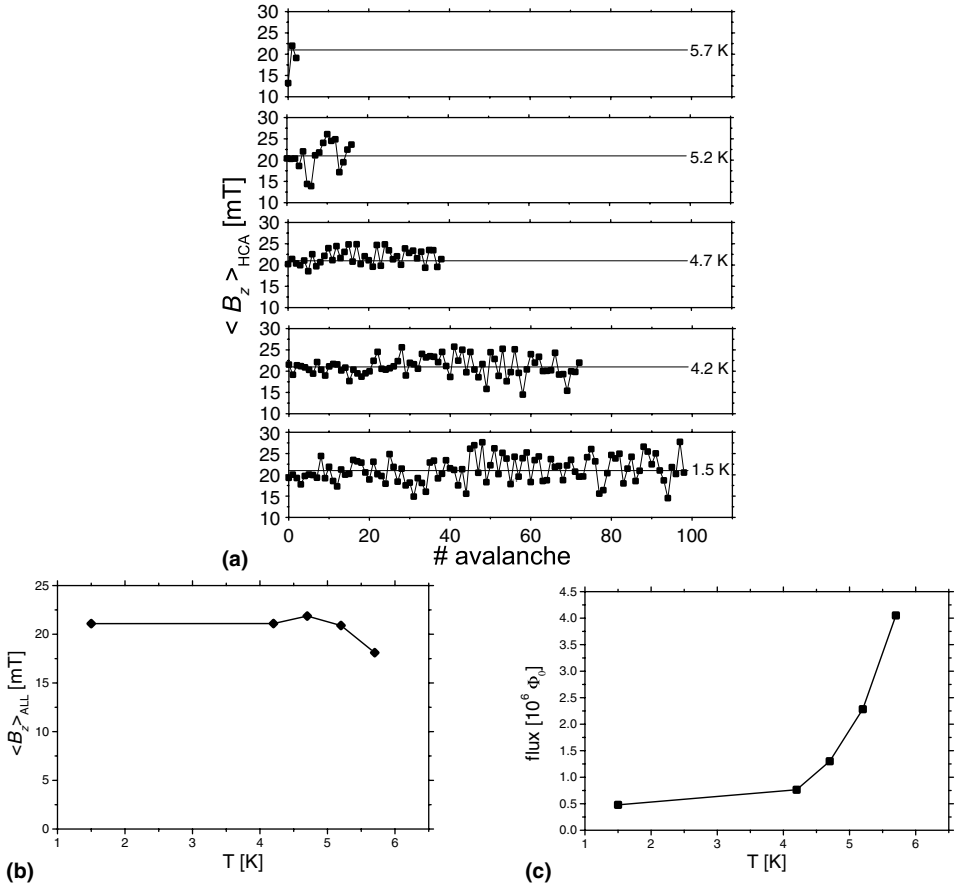

Fig. 4. (a) Average magnetic induction $\langle B_z \rangle_{\mathrm{HCA}}$ for each individual observed HCA in the temperature range (1.5 K $\leqslant T \leqslant$ 5.7 K). The individual HCAs are registered as separate events indicated by an index along the x-axis. (b) Plot of the magnetic induction $\langle B_z \rangle_{\mathrm{ALL}}$ averaged over all measured avalanches. Independent of temperature, we find $\langle B_z \rangle_{\mathrm{ALL}} \approx 21$ mT. (c) Average flux in a HCA (averaged over all HCAs) as a function of temperature.

lanches occur. The increase with temperature of the HCA size S expressed as the average flux in a single HCA, is shown in Fig. 4c.

Another property which characterizes the HCAs is the applied field where the first HCA occurs. This threshold field is often called [4] first jump field B_{fj}. We determine B_{fj} as a function of the reduced temperature T/T_{c} resulting in the 'phase diagram' of Fig. 5. The filled circles correspond to the first jump field B_{fj} below which we do not observe HCAs, while above B_{fj} HCA are present. To illustrate that the HCA structure becomes larger and more branched, we also show some of the typical observed HCA structures, which are all shown using the same magnification. For $T/T_{\mathrm{c}} \gtrsim 0.67$, no HCAs are present and flux penetration takes place in a regular manner.

3.2. Substrate orientation

We now discuss the influence of substrate orientation to try and explain the large qualitative difference in behavior of samples that were grown on either A- or R-plane sapphire substrates. Contrary to the rather compact and huge flux jumps of the A-plane samples discussed above, in R-plane samples much smaller and more fractal avalanches are observed [15]. It is interesting to compare the

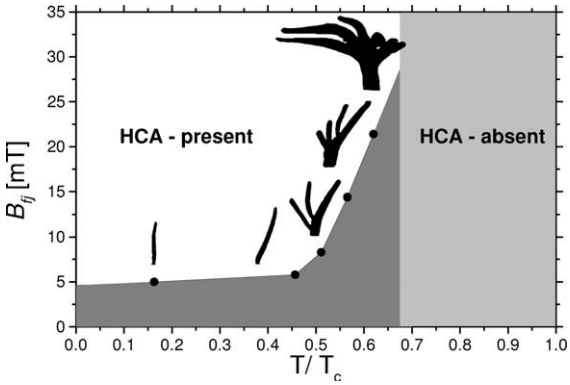

Fig. 5. 'Phase diagram' for the flux penetration patterns in Nb thin films on *A*-plane sapphire substrates. The filled circles indicate the first jump field B_{fj}, the onset of the regime where HCAs are present. Above $T/T_c \sim 0.67$ no HCA are observed. In this plot some of the typical observed HCA shapes are shown in black. With increasing temperature, the HCA structure becomes larger and more branched.

flux penetration at 6.2 K (where HCAs are absent) for two samples which apart from substrate orientation are identical. In Fig. 6, we show the average flux penetration profiles $\langle B_z(x,y)\rangle_x$ in both samples at 6.2 K and applied field $\mu_0 H = 2$ mT. Clearly, flux penetration in the *R*-plane sample is much faster and the critical current (roughly the slope of the curve) is much lower. It might well be that due to the lower critical current in the *R*-plane case, the sample is subcritical for thermal runaway, and that therefore we do not observe HCAs (in the investigated temperature regime) for such samples.

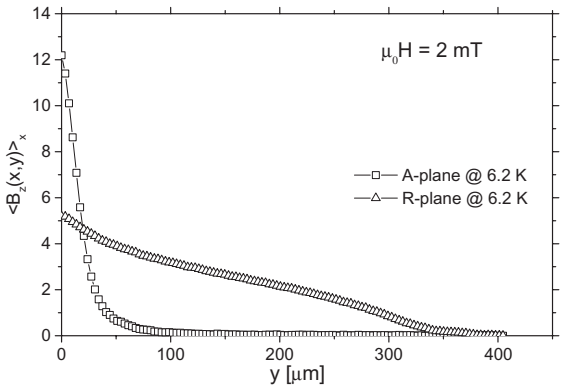

Fig. 6. Average magnetic flux profile $\langle B_z(x,y)\rangle_x$ in samples on *A*- and *R*- plane sapphire substrates at an applied field of 2 mT. Clearly, flux penetration in the *R*-plane sample goes much faster and the critical current is much smaller.

4. Summary

Using an advanced magneto-optical technique to study HCAs in niobium thin films on *A*-plane sapphire substrates in the range of $1.5\ \mathrm{K} \leqslant T \leqslant T_c = 9.2$ K, we find that HCAs do not reproduce from experiment to experiment on a detailed level. With increasing temperature we find more branching of the HCAs resulting in a more irregular flux pattern. We determine the applied field at which the first HCA occurs. At higher temperatures, the number of HCAs decreases and more 'regular' flux penetration starts to dominate the behavior. Above 6.2 K no HCAs are observed anymore. The average magnetic field in the HCAs remains constant at ≈21 mT up to 5.5 K. Our observations are in agreement with numerical simulation results of Aranson et al. [14] making a thermo-magnetic origin of this phenomenon likely. From the observed difference in flux penetration and critical current, we conjecture that samples on *R*-plane sapphire are subcritical to thermal runaway (for the investigated temperature regime) which explains why in these samples no HCAs are observed. This connection between HCAs and high critical current implies that for technological applications, where one pursuits high critical currents, it is worthwhile to search for solutions such as improvement of the heat conductivity [4] of the sample or substrate.

5. Acknowledgments

We would like to thank C.M. Aegerter for useful discussions concerning the analysis. This work was supported by FOM (Stichting voor Fundamenteel Onderzoek der Materie), which is financially supported by NWO (Nederlandse Organisatie voor Wetenschappelijk Onderzoek).

References

[1] R.P. Huebener, V.A. Rowe, R.T. Kampwirth, J. Appl. Phys. 41 (1970) 2963.

[2] R.V. Bujok, P. Brüll, J. Boneberg, S. Herminghaus, P. Leiderer, Appl. Phys. Lett. 63 (1993) 412;
U. Bolz, D. Schmidt, B. Biehler, B.-U. Runge, R.G. Mints, K. Numssen, H. Kinder, P. Leiderer, Physica C 388–389 (2003) 715.

[3] M. Baziljevich, A.V. Bobyl, D.V. Shantsev, E. Altshuler, T.H. Johansen, S.I. Lee, Physica C 369 (2002) 93.

[4] A.V. Bobyl, D.V. Shantsev, T.H. Johansen, W.N. Kang, H.J. Kim, E.M. Choi, S.I. Lee, Appl. Phys. Lett. 80 (2002) 4588.

[5] F.L. Barkov, D.V. Shantsev, T.H. Johansen, P.E. Goa, W.N. Kang, H.J. Kim, E.M. Choi, S.I. Lee, Phys. Rev. B 67 (2003) 064513.

[6] S.S. James, S.B. Field, J. Seigel, H. Shtrikman, Physica C 332 (2000) 445.

[7] E.R. Nowak, O.W. Taylor, L. Liu, H.M. Jaeger, T.I. Selinder, Phys. Rev. B 55 (1997) 11702.

[8] K. Behnia, C. Capan, D. Mailly, B. Etienne, Phys. Rev. B 61 (2000) R3815;
J. Magn. Magn. Mater. 226 (2001) 370.

[9] E. Altshuler, T.H. Johansen, Y. Paltiel, P. Jin, K.E. Bassler, O. Ramos, G.F. Reiter, E. Zeldov, C.W. Chu, <cond-mat/0208266>.

[10] R. Aoki, H.U. Habermeier, Jpn. J. Appl. Phys. 26 (1987) 1453.

[11] V.A. Rowe, R.P. Huebener, R.T. Kampwirth, Phys. Stat. Sol. (a) 4 (1971) 513.

[12] C.A. Duran, P.L. Gammel, R.E. Miller, D.J. Bishop, Phys. Rev. B 52 (1995) 75.

[13] C.P. Bean, Rev. Mod. Phys. 36 (1964) 31.

[14] I. Aranson, A. Gurevich, V. Vinokur, Phys. Rev. Lett. 87 (2001) 067003.

[15] M.S. Welling, C.M. Aegerter, R.J. Westerwaal, S. Enache, R.J. Wijngaarden, R. Griessen, Physica C 406 (2004) 100.

[16] R.J. Wijngaarden, K. Heeck, M. Welling, R. Limburg, M. Pannetier, K. van Zetten, V.L.G. Roorda, A.R. Voorwinden, Rev. Sci. Instrum. 72 (2001) 2661.

[17] L.A. Dorosinskii, M.V. Indenbom, V.I. Nikitenko, Y.A. Ossipyan, A.A. Polyanskii, V.K. Vlasko-Vlasov, Physica C 203 (1992) 49.